Synthesis, structure–activity relationships and molecular modeling studies of new indole inhibitors of monoamine oxidases A and B

ARTICLE *in* BIOORGANIC & MEDICINAL CHEMISTRY · NOVEMBER 2008

Impact Factor: 2.79 · DOI: 10.1016/j.bmc.2008.09.072 · Source: PubMed

8 AUTHORS, INCLUDING:

Romano Silvestri
Sapienza University of Rome
118 PUBLICATIONS **2,173** CITATIONS
SEE PROFILE

Antonio Lavecchia
University of Naples Federico II
118 PUBLICATIONS **2,415** CITATIONS
SEE PROFILE

Ettore Novellino
University of Naples Federico II
610 PUBLICATIONS **8,828** CITATIONS
SEE PROFILE

Bioorganic & Medicinal Chemistry 16 (2008) 9729–9740

Contents lists available at ScienceDirect

Bioorganic & Medicinal Chemistry

journal homepage: www.elsevier.com/locate/bmc

Synthesis, structure–activity relationships and molecular modeling studies of new indole inhibitors of monoamine oxidases A and B

Giuseppe La Regina [a], Romano Silvestri [a,*], Valerio Gatti [a], Antonio Lavecchia [b,*], Ettore Novellino [b], Olivia Befani [c], Paola Turini [c], Enzo Agostinelli [c]

[a] Istituto Pasteur – Fondazione Cenci Bolognetti, Dipartimento di Chimica e Tecnologie del Farmaco, Sapienza Università di Roma, Piazzale Aldo Moro 5, I-00185 Roma, Italy
[b] Dipartimento di Chimica Farmaceutica e Tossicologica, Università di Napoli Federico II, Via Domenico Montesano 49, I-80131 Napoli, Italy
[c] Dipartimento di Scienze Biochimiche Rossi-Fanelli and Istituti di Biologia e Patologia Molecolare del CNR, Sapienza Università di Roma, Piazzale Aldo Moro 5, I-00185 Roma, Italy

ARTICLE INFO

Article history:
Received 20 June 2008
Revised 25 September 2008
Accepted 30 September 2008
Available online 2 October 2008

Keywords:
Amine oxidase
Monoamine oxidase type A
Monoamine oxidase type B
Indole
Structure–activity relationships
Molecular modeling
Molecular dynamics

ABSTRACT

New monoamine oxidase inhibitors were synthesized as indole analogues of a previously reported pyrrole series. Several compounds were potent MAO-A (**12**, **17**, **19–22**, **31**, **36**, and **37**) or MAO-B (**14**, **20**, **24**, **38**, **44**, and **46**) inhibitors, and had K_i values in the nanomolar concentration range. In particular, **22** (K_i = 0.00092 μM, and SI = 68,478) was exceptionally potent and selective as MAO-A inhibitor. In molecular modeling studies, compounds **22**, **24**, **44**, and **46** positioned the indole ring into an aromatic cavity of MAO-A, and established π–π stacking interactions with Tyr407, Tyr444, and FAD cofactor. However, only compound **22** was able to form hydrogen bonds with FAD, a finding which was in accordance with its potent anti-MAO-A activity. Conversely, **22**/MAOB complex was highly unstable during the MD simulation.

1. Introduction

Monoamine oxidases (MAOs) catalyze the oxidative catabolism of biogenic amines.[1] MAO-A and MAO-B are the isoforms of MAOs present in most mammal tissues; they are often bound to the outer mitochondrial membrane, but differ with respect to amino acid sequence, distribution in body's tissues, and substrate/inhibitor specificity.[2] MAO-A preferentially deaminates serotonin (5-HT), adrenaline (A) and noradrenaline (NA), and is selectively inhibited by clorgyline (**1**) and moclobemide (**2**). MAO-B catalyzes the oxidative deamination of β-phenylethylamine and benzylamine, and is selectively inhibited by selegiline (L-deprenyl, **3**). Dopamine (DA) in vitro, and tyramine are deaminated by both isoforms, but human DA is preferentially deaminated by MAO-B.

MAO-A and MAO-B are attractive targets for therapeutic intervention. MAO-A inhibitors are prescribed for the treatment of mental depression and anxiety.[3] MAO-B inhibitors are used with L-DOPA and/or DA agonists in the symptomatic treatment of Parkinson's disease (PD).[4] MAO inhibitors are also used in combination (i.e., a MAO-A (**2**) plus a MAO-B (lazabemide, (**4**) reversible inhibitors) to treat therapy-resistant depression.[5] Ladostigil (**5**, *R*-isomer) combines the structural features of rivastigmine (acetylcholinesterase inhibitor) and rasagiline (MAO-B inhibitor), and is potentially useful for Alzheimer's (AD) disease, Lewy Body disease, and eventually PD.[6] M-30 (**6**) is a brain selective agent characterized by the presence of both propargyl anti-MAO and iron-chelating moieties; it might serve as drug for neurodegenerative disorders, such as PD and AD, in which oxidative stress and iron alteration are implicated.[7]

Previously, we designed a new class of potent and selective pyrrole MAO inhibitors by means of a simple model derived from the structures **2** and **3**.[8] The synthesis of new pyrrole analogues allowed to determine the structure–activity relationships (SARs) and features of the MAO-A/B selectivity, and led to disclose highly selective MAO-B (**7**, SI = 0.0057) and MAO-A (**8**, SI = 12,500) inhibitors.[9]

As a progress of this research project, we here describe the synthesis of new indole derivatives. The indole nucleus is the key feature of potent anti-MAO agents (i.e., the MAO-B inhibitor PF9601N (**9**) shows antioxidant/neuroprotective properties in an experimental model of PD[10,11]; **10** is a potent MAO-A inhibitor of a member a series of indolymethylamines derived from tryptamine).[12]

* Corresponding authors. Tel.: +39 06 4991 3800; fax: +39 06 491 491 (R.S.); tel./fax: +39 081 678 613 (A.L.).
E-mail addresses: romano.silvestri@uniroma1.it (R. Silvestri), lavecchi@unina.it (A. Lavecchia).

0968-0896/$ - see front matter © 2008 Elsevier Ltd. All rights reserved.
doi:10.1016/j.bmc.2008.09.072

According to our previous findings,[8,9] the MAO-A/B selectivity of **11–50** was dependent on small modifications of the chemical structure. Molecular modeling studies carried out using our previously reported model,[9] allowed to clarify the binding mode of the most active inhibitors **22, 24**, **44**, and **46** (see Chart 1).

2. Results

2.1. Chemistry

Reaction of indole-2-carboxylic acid with appropriate amines at room temperature in the presence of (benzotriazol-1-yloxy)tris(dimethylamino)phosphonium hexafluorophosphate (BOP) and triethylamine in anhydrous DMF afforded amides **11–13**, **15**, **16**, **18**, **19**, **21–23**, **25**, **26**, **41**, and **43–46**. Compounds **12**, **16**, **19**, **22**, and **25** were alkylated with iodomethane by phase-transfer reaction in the presence of tetrabutylammonium hydrogen sulfate (TBAHS) in 50% sodium hydroxide solution and dichloromethane to give **14**, **17**, **20**, **24**, and **27**, respectively.

Lithium aluminum hydride reduction of amides **11–14**, **16**, **17**, **19, 20, 22**, **24**, **25**, **41**, and **43–46** in refluxing tetrahydrofuran furnished amines **28–31**, **33**, **34**, **36–42**, and **47–50**, respectively (Scheme 1). Commercially available amines **51–54** were transformed into the corresponding carbamates **55–58** by reaction with ethyl chloroformate in the presence of triethylamine in anhydrous tetrahydrofuran. **55–58** were reduced to amines **59–62** with lithium aluminum hydride (Scheme 2).

2.2. Biology

Bovine brain mitochondria isolated according to Basford[13] were used as source of the two MAO isoforms. Compounds **1–3**, **7**,[8] and **8**[8] were used as reference drugs. MAO-A and MAO-B activities were determined by a fluorometric assay, using kynuramine as a substrate, in the presence of their specific inhibitors (L-deprenyl 1 μM for MAO-A, and clorgyline 1 μM for MAO-B).[14] The four final concentrations ranged from 5 μM to 0.1 mM. Dixon plots showed that the inhibition was not competitive (an example is shown in Supplementary data). The inhibitory activities (K_i) and A-selectivity (SI) of compounds **11–50** are depicted in Table 1.

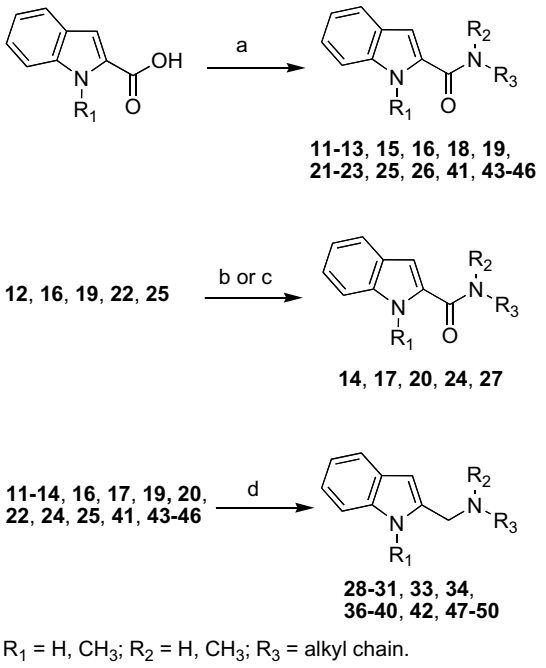

Scheme 1. Synthesis of Derivatives **11**–**50**. Reagents and reaction conditions: (a) amine, BOP, triethylamine, anhydrous DMF, 25 °C, 4 h; (b) (**14**, **17**, **20**, and **24**), iodomethane (6 equiv), TBAHS, 50% NaOH, dichloromethane, room temperature, 25 °C, 3 h; (c) (**27**) iodomethane (12 equiv), TBAHS, 50% NaOH, dichloromethane, room temperature, 25 °C, 48 h; (d) lithium aluminum hydride, anhydrous THF, reflux, overnight.

All compounds were reversible inhibitors; the enzyme activity (approx. 95–100%) was restored after 24 h dialysis at 5 °C (dialysis was performed in the presence of 0.1 M potassium phosphate buffer at pH 7.2). Because of the high affinity of the inhibitors, no dissociation of the enzyme–inhibitor complex was detected during

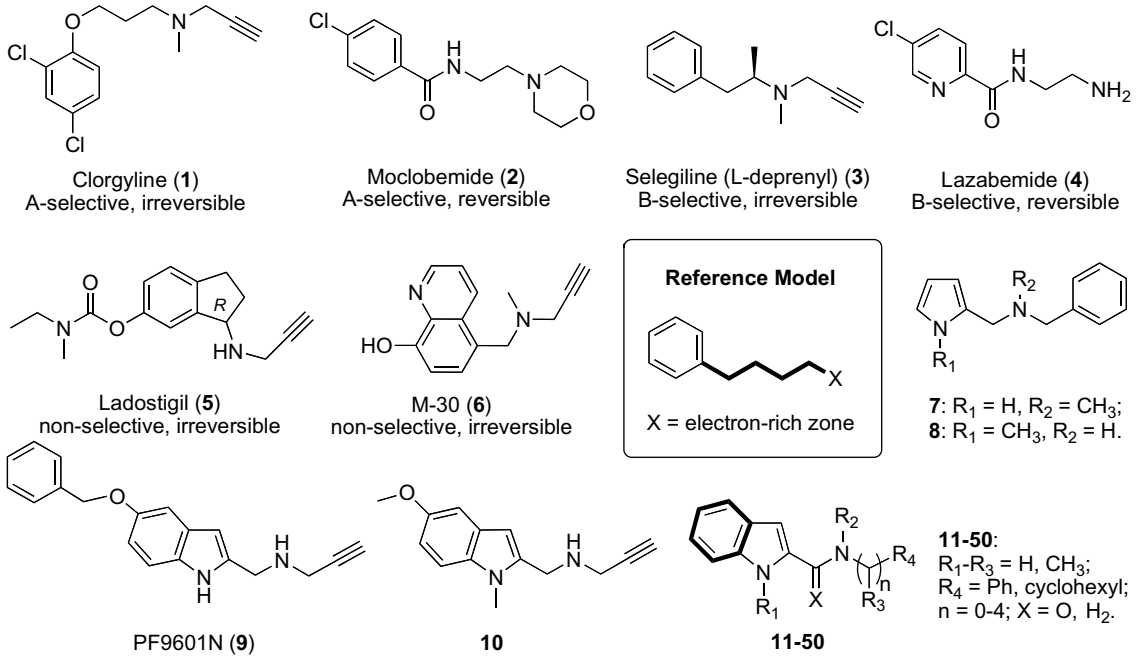

Chart 1. Structure of references **1**–**10** and new MAO inhibitors **11**–**50**.

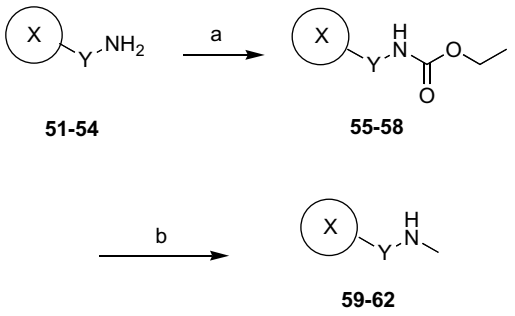

51, **55**, **59**: X = phenyl, Y = $(CH_2)_3$; **52**, **55**, **60**: X = phenyl, Y = $(CH_2)_4$; **53**, **57**, **61**: X = cyclohexyl, Y = (*R*)-$CH(CH_3)$; **54**, **58**, **62**: X = cyclohexyl, Y = (*S*)-$CH(CH_3)$.

Scheme 2. Synthesis of derivatives **59**–**82**. Reagents and reaction: (a) ethyl chloroformate, triethyamine, anhydrous THF, 25 °C, 2 h; (b) lithium aluminum hydride, anhydrous THF, reflux, overnight.

the enzymatic activity assay, and the inhibition was apparently irreversible. In these experimental conditions the substrate did not compete with the inhibitor. Accordingly, a decrease of V_{max} was observed, while the K_m value was unchanged.

2.3. Discussion

The majority of tested compounds inhibited MAO-A at submicromolar concentration, and compounds **12**, **17**, **19–22**, **31**, **36**, and **37** had K_i values in the nanomolar range. Several compounds inhibited MAO-B at micromolar concentration, and five compounds (**14**, **20**, **24**, **38**, **44**, and **46**) had K_is in the low nanomolar range. The selectivity indexes (SIs) ranged from 68,478 (**22**) to 0.034 (**24**).

Generally, the carboxamides were potent MAO-A inhibitors. *N*-methyl, *N*-(3-phenyl)propyl carboxamide (**22**) was found an exceptionally potent MAO-A inhibitor (K_i(MAO-A) = 0.00092 μM); worthy to note, this compound was 8-fold more potent than corresponding pyrrole analogue (K_i(MAO-A) = 0.007 μM).[8] Introduction of a methyl group at position 1 of the indole of **22** provided **24**, a compound endowed with higher MAO-B inhibitory activity but low selectivity. Reduction of the carbonyl functionality to a methylene of either **22** or **24** resulted in reduction of anti-MAO-A activity and selectivity (compounds **38** and **39**). N-methylation of carboxamides **11**, **18**, and **21** improved the anti-MAO-A activity (compare **11** with **12** (K_i(MAO-A) = 0.0035 μM), **18** with **19** (K_i(MAO-A) = 0.004 μM), and **21** with **22** (K_i(MAO-A) = 0.00092 μM)). The anti-MAO-A activity of **16** increased 12 times by introduction of a methyl group at position 1 of the indole (compare **16** with **17** (K_i(MAO-A) = 0.006 μM)).

Reduction of the carbonyl functionality of **11–27** resulted in a dramatic drop of MAO-A inhibition, and only **33** and **36** retained the activity of the parent compounds **16** and **19**, respectively. As MAO-B inhibitor, amine **28** (K_i(MAO-B) = 0.32 μM) was as active as carboxamide **11** (K_i(MAO-B) = 0.23 μM), and amines **36** (K_i(MAO-B) = 0.02 μM) and **38** (K_i(MAO-B) = 0.025 μM) were more potent than carboxamides **19** and **22**, respectively. Replacement of the pyrrole nucleus of **7** with the indole (**33**) led to 35 times abatement of anti-MAO-B activity and loss of selectivity.

The most potent MAO-A (**22**, K_i(MAO-A) = 0.00092 μM) and MAO-B (**24**, K_i(MAO-B) = 0.0015 μM) inhibitors had the same spacer group. Reference inhibitors **7** and **8**[9] also have the same spacer group which differs from the spacer group of compounds **22** and **24** in (i) linker chain length (propyl for indoles **22** and **24**, and methylene for pyrroles **7** and **8**), (ii) functional group (indoles **22** and **24** are carboxamides, and pyrroles **7** and **8** are amines). Compound **22** is a potent and selective MAO-A inhibitor, and derivative **24** is a potent but not selective inhibitor of the MAO-B. Carboxamides **44** and **46** were potent but not selective MAO inhibitors. Worthy to note, these compounds are (*S*)-enantiomers, while in the pyrrole series[9] the highest inhibition was due to the corresponding (*R*)-enantiomers. Reduction of carboxamides **44** and **46** to the corresponding amines **48** and **50** resulted in reduction of both MAO-A and MAO-B inhibitory activity.

2.4. Molecular modeling

X-ray crystal structures of rat MAO-A (PDB code: 1O5W)[15] and human MAO-B (PDB code: 1OJC)[16,17] were used for docking experiments.[9] The rat, human and bovine sequences at the catalytic site show high level of identity.[18] In particular, the rat and bovine sequences of MAO-A are characterized by 85.3% of identity and 95.4% of homology at the binding site, while the human and bovine sequences of MAO-B have 91.3% of identity and 97.1% of homology. The residues of the active site are largely conserved across the MAO isoforms and only one mutation is found at the catalytic site of the human and bovine MAO-B (Ile199 is replaced by Phe199). Consequently, in order to simulate the active site of the bovine MAO-B, the 1OJC crystal structure was virtually mutated, replacing the Ile199 with a Phe residue.

Four water molecules, labeled as WAT23, WAT82, WAT102, and WAT160 according to the numbering reported in the human MAO-B crystallographic structure (PDB code: 1OJC),[16,17] were located near the FAD cofactor, this latter being covalently bound to Cys397. WAT102 and WAT23 were already detected in the crystallographic analysis of hMAO-B:[16,17] WAT160 was found below the FAD pyrimidine ring, fixed by the π-systems of the aromatic side chains of Tyr398 and Tyr435, as well as by the central heterocyclic conjugated ring of FAD. WAT82 was positioned about 3.70 Å away from the α carbons of Ile198 and Gln206. Accordingly, we considered these water molecules as integral components of the protein structure during the docking simulations.

Docking studies focused on the most active and/or selective inhibitors **22**, **24**, **44**, and **46**, using the automated docking program GOLD 3.1.[19–24] GOLD provides accurate prediction of ligand binding conformation, while the GOLD scoring function (i.e., GOLD fitness) is not parameterized for small molecule binding affinities. Recently, Verdonk et al.[25] reported *GOLDscore* as a modified GOLD scoring function (is equal to the GOLD fitness minus the ligand intramolecular terms). *GOLDscore* provides a better correlation with the experimental binding affinities. Indeed, correlation statistics from *GOLDscore* are comparable to those obtained from Chemscore function, which is parameterized against experimental binding affinities. In order to assess the reliability of predicted binding models, the estimated *GOLDscore* values for the top-ranked solutions of **22**, **24**, **44**, and **46** were compared with the experimental MAO inhibitory activities (pK_is). *GOLDscore* function implemented in GOLD surprisingly approximated in a qualitative sense the experimental binding affinities (Table 2).

To evaluate the dynamic stability of the predicted ligand/enzyme interactions, the complexes obtained from docking were submitted to molecular dynamics (MD) simulation for 600 ps at constant temperature (300 K). The relative dynamic stability of each ligand docked conformation was monitored by the root-mean-squared deviations (rmsd) of the ligands relative to their initial docked orientation, and by the enzyme–ligand H-bond distance time series along the complete 600 ps MD trajectory.

Docking of compounds **22** (*GOLDscore* = 54.95 kJ/mol), **24** (*GOLDscore* = 53.31 kJ/mol), **44** (*GOLDscore* = 43.00 kJ/mol), and **46** (*GOLDscore* = 44.58 kJ/mol) to the rat MAO-A clearly showed one prevailing pose into the active site (Fig. 1a–d). The top-ranking results from GOLD runs placed the indole ring of the ligands within

Table 1
Structures and monoamine oxidase inhibitory activities of derivatives **11**–**50**

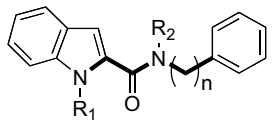

11-27

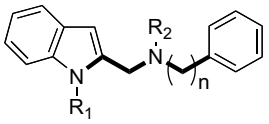

28-40

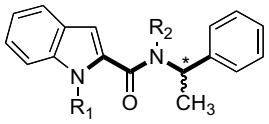

41

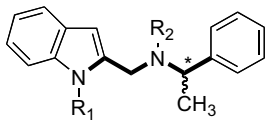

42

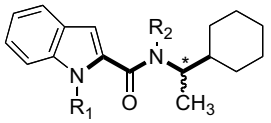

43-46

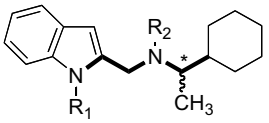

47-50

Compound	R_1	R_2	*n*	*	K_i (μM) MAO-A	K_i (μM) MAO-B	SI[a]
11	H	H	0	—	0.13	0.23	1.8
12	H	CH_3	0	—	0.0035	0.094	26.8
13	CH_3	H	0	—	10	>100	>10
14	CH_3	CH_3	0	—	0.015	0.021	1.4
15	H	H	1	—	0.03	0.12	4.0
16	H	CH_3	1	—	0.07	1.6	22.9
17	CH_3	CH_3	1	—	0.006	0.96	160.8
18	H	H	2	—	0.17	0.19	1.1
19	H	CH_3	2	—	0.004	0.1	25
20	CH_3	CH_3	2	—	0.0065	0.037	5.69
21	H	H	3	—	0.005	0.8	160
22	H	CH_3	3	—	0.00092	63	68478
23	CH_3	H	3	—	0.1	>100	>1000
24	CH_3	CH_3	3	—	0.044	0.0015	0.034
25	H	H	4	—	2.2	10.0	4.5
26	H	CH_3	4	—	10	>100	>10
27	CH_3	CH_3	4	—	1.0	8.3	8.3
28	H	H	0	—	10	0.32	0.032
29	H	CH_3	0	—	0.01	1.0	100.0
30	CH_3	H	0	—	0.01	75.0	7500.0
31	CH_3	CH_3	0	—	0.006	11.0	1833.3
32	H	H	1	—	2.1	>100	>47
33	H	CH_3	1	—	0.06	0.7	11.6
34	CH_3	CH_3	1	—	7.2	9.7	1.3
35	H	H	2	—	1.6	>100	>62.5
36	H	CH_3	2	—	0.001	0.02	20.0
37	CH_3	CH_3	2	—	0.007	25	3571.4
38	H	CH_3	3	—	0.073	0.025	0.34
39	CH_3	CH_3	3	—	0.089	0.93	10.4
40	H	H	4	—	10	>100	>10
41	H	H	—	*R,S*	0.25	0.5	2
42	H	H	—	*R,S*	10	>100	>10
43	H	CH_3	—	*R*	0.77	23	29.8
44	H	CH_3	—	*S*	0.012	0.016	1.3
45	CH_3	CH_3	——	*R*	0.70	92	131.4
46	CH_3	CH_3	—	*S*	0.054	0.015	0.27
47	H	CH_3	—	*R*	0.01	5.9	590.0
48	H	CH_3	—	*S*	0.06	0.03	0.5
49	CH_3	CH_3	—	*R*	9.8	5.3	0.5
50	CH_3	CH_3	—	*S*	0.065	0.1	1.5
1[b]	—	—	—	—	0.054	58	1074.1
2[b]	—	—	—	—	11.5	>100	>87
3[b]	—	—	—	—	3.8	0.97	0.25
7[b]	—	—	—	—	3.5	0.02	0.0057
8[b]	—	—	—	—	0.024	300	12,500.0

Data represent mean values for at least three separate experiments each performed in duplicate. Standard errors were within 2%.
[a] SI, selectivity index = K_i(MAO-B)/K_i(MAO-A) ratio.
[b] Lit.[8].

an 'aromatic cage', so that it forms π–π stacking interactions with Tyr407 and Tyr444 side chains, as well as with the isoalloxazine FAD ring, while the aromatic or cyclohexyl rings were located in a hydrophobic core delimited by residues Phe208, Val210, Ile325, and Leu337. In particular, the aromatic ring of **22** and **24** established a π-stacking interaction with Phe208 (Fig. 1a and b). With the only exception of **22**, which formed two H-bonds with N5 nitrogen and C=O4 oxygen of FAD by its indole NH (Fig. 1a), GOLD did not detect any H-bond in the enzymatic cleft for the remaining compounds. The high MAO-A affinity and A/B selectivity of **22** might therefore be accounted by the formation of these two H-bonds. Worthy to note, the binding mode of **24**, **44**, and **46** strongly resembled that of **22**, with the exception of the indole ring which was rotated of 180° so that it projected the methyl group on the opposite side of the cofactor (Fig. 1b and d).

To explore the dynamic stability of **22**, **24**, **44**, and **46** in complex with MAO-A, rmsd values for the enzyme Cα atoms during the production phase (300 ps) relative to the starting structures

Table 2
Docking scores of compounds **22**, **24**, **44**, and **46** by *GOLDscore* in the GOLD software, and experimental MAO-A and MAO-B inhibitory activities (pK_i)

Ligand	Enzyme	N_{tot}[a]	*GOLDscore*[b] (kJ/mol)	pK_i (μM)
22	MAO-A	5	54.95	9.0
24	MAO-A	6	53.31	8.8
44	MAO-A	9	43.00	7.9
46	MAO-A	3	44.58	7.3
22	MAO-B	4	22.00	4.2
24	MAO-B	10	43.56	8.8
44	MAO-B	4	33.45	7.8
46	MAO-B	5	29.98	7.8

[a] N_{tot} is the total number of docking poses generated by GOLD after 20 runs.
[b] *GOLDscore* represents the GOLD fitness minus intramolecular terms.[25]

were calculated. The rmsd plots (data not shown) indicated that the conformations of the four complexes achieved equilibrium after about 100 ps and that their average rmsd were 1.60 Å, 1.65 Å, 1.70 Å, and 1.75 Å, respectively. This behavior reveals that the overall architectures of the macromolecular complexes were preserved for the whole duration of the simulations. Moreover, the H-bonds between the indole NH of **22** and N5 nitrogen and C=O4 oxygen of FAD were maintained throughout the MD simulation with a frequency of formation of 87% and 65%, respectively (Fig. 2). A weak H-bond between the amide C=O oxygen of **22** and Gln215 NH was also observed (47%).

MD trajectories of **24** and **44** showed two stable H-bonds formed between the C=O oxygen of **24** and the OH hydrogen of Tyr298 (82%), and between the indole NH of **44** and the C=O oxygen of Asn181 (70%). No intermolecular H-bonds were detected by analyzing the MD trajectory of **46**/MAO-A complex. The π–π stacking interactions involving the ligand phenyl and benzo-fused indole rings and Phe208, Tyr444, and Tyr407 were also preserved during the entire MD simulation. These findings suggest that the superior MAO-A inhibitory activity of **22** compared with **24**, **44**, and **46** is regulated by its ability to form close and productive interactions with FAD.

The MAO-B active site consists of two cavities, the substrate cavity in front of the flavin and the entrance cavity located underneath the protein surface and closed by the loop formed by residues 99–112. Compounds **22**, **24**, **44**, and **46** easily fit into the MAO-B active site with two prevailing binding modes (Fig. 3a–d). The best scored docking poses of **22** (*GOLDscore* = 22.00 kJ/mol), **44** (*GOLDscore* = 33.45 kJ/mol) and **46** (*GOLDscore* = 29.98 kJ/mol) occupied both the cavities (Fig. 3a, c, and d).

In particular, the indole system was hosted in the entrance cavity made up by lipophilic residues Pro104, Phe168, Leu164, Leu171, Phe199, Ile326, whereas the phenyl or cyclohexyl rings occupied the substrate cavity and were in direct contact with the isoalloxazine FAD ring, Tyr398, Tyr435, Phe343, and Tyr60. Worthy to note, the phenyl ring of **22**, differently from that of **44** and **46**, adapted itself just underneath the enzyme 'aromatic cage' and seemed unable to establish any charge-transfer interaction with the enzyme. All three compounds established a H-bond with Gln206 NH_2 by their amide C=O oxygen. In addition, compounds **22** and **44** had their NH indole involved in a H-bond with Tyr326 OH oxygen, whereas compounds **44** and **46** engaged a H-bond with WAT82 by their amide C=O oxygen. As far as regarded compound **24**, GOLD detected a different binding mode (*GOLDscore* = 43.56 kJ/mol), which closely resembled that of **22, 24, 44**, and **46** into the MAO-A binding cleft (Fig. 3b). The indole was in front of the FAD isoalloxazine ring, while the phenyl ring was lodged in a hydrophobic pocket framed by residues Phe168, Trp119, Phe103, Pro104, Ile316, and Phe199; no intermolecular H-bonds between ligand and enzyme were observed.

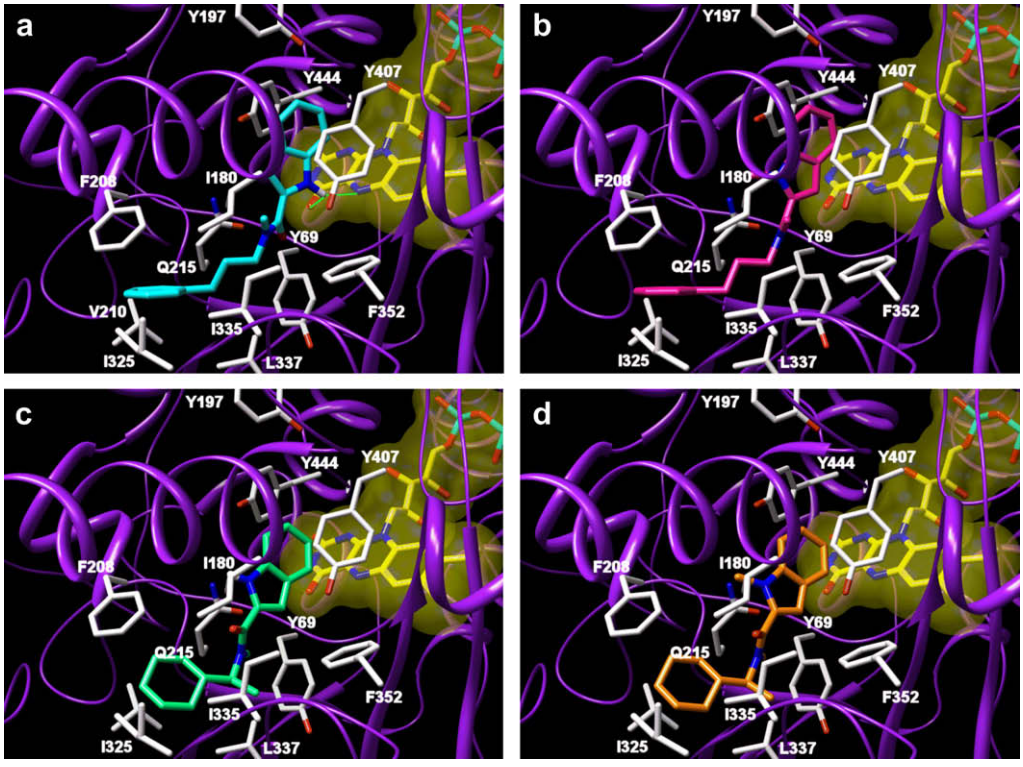

Figure 1. Binding modes of compounds **22** (cyan, a), **24** (magenta, b), **44** (spring green, c) and **46** (orange, d) into the MAO-A binding cavity. For clarity, only interacting residues are displayed. Ligands, FAD cofactor (yellow) and interacting key residues (white) are represented as stick models, while the enzyme (violet) as ribbons. The van der Waals volume of FAD is displayed as a transparent yellow surface. H-bonds are shown as green lines.

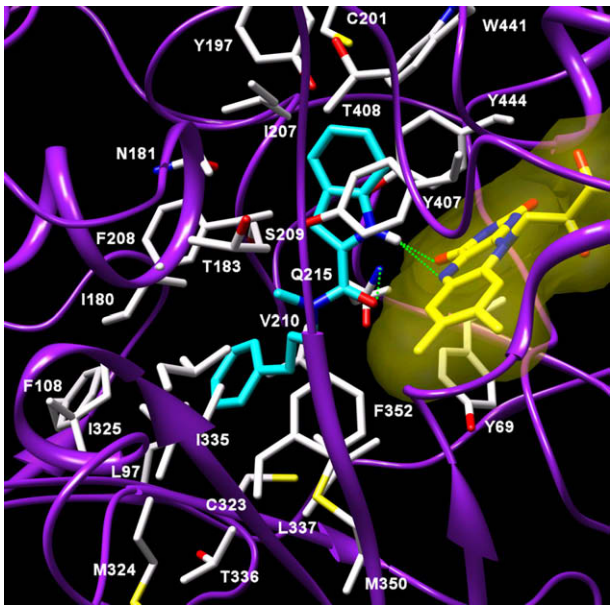

Figure 2. MD snapshot of **22**/MAO-A complex. Only aminoacids located within a 5 Å distance of the bound ligand are displayed and labeled. Carbon atoms of **22** and cofactor FAD are cyan and yellow, respectively. The van der Waals volume of FAD is displayed as a transparent yellow surface. The hydrogen bonds discussed in the text are depicted as dashed green lines.

MD studies of **22**, **24, 44**, and **46**/MAO-B complexes were carried out in order to assess their dynamic stability. The average rmsd of the backbone Cα atoms with respect to the initial structure revealed a quite stable behavior in the **24**/MAO-B (1.2 Å), **44**/MAO-B (1.0 Å), and **46**/MAO-B (1.1 Å) complexes. Analysis of the MD trajectories of **24**/MAO-B complex showed that the ligand was mainly stabilized by hydrophobic and π−π stacking interactions: the *N*-methyl indole moiety was embedded in the 'aromatic cage', where it established π−π stacking and T-shaped interactions with Phe343, Tyr60, and Tyr435; the phenyl moiety made a strong π−π interaction with Phe199, which turned out very stable throughout the whole MD simulation.[6b] Although the H-bond between the indole NH of **44** and Tyr326 OH oxygen was broken during the simulation, both **44** and **46** preserved their H-bonds with both Gln206 and WAT82. In contrast, **22**/MAO-B complex showed a remarkably different behavior. In fact, during the MD simulation, **22** was highly unstable, and moved away from the FAD cofactor after a few hundreds of ps. The most important interactions with the enzyme residues failed and the final Cα atom rmsd values were equal to 3.1 Å. This implies that compound **22** compared with **24, 44**, and **46** undergoes larger conformational changes after complex formation, which reflects its very weak MAO-B binding affinity.

3. Conclusions

New monoamine oxidase inhibitors were synthesized as indole analogues of a previously reported pyrrole series. Several compounds were potent MAO-A (**12**, **17**, **19–22**, **24**, **31**, **36**, and **37**) or MAO-B (**14**, **20**, **24**, **38**, **44**, and **46**) inhibitors, and had K_i values in the nanomolar concentration range. In particular, **22** (K_i = 0.00092 μM, and SI = 68,478) was exceptionally potent and selective as MAO-A inhibitor. Molecular modeling studies showed that compounds **22**, **24**, **44**, and **46** positioned the indole ring into an 'aromatic cage' of MAO-A, and formed π−π stacking interactions with Tyr407 and Tyr444 side chains, as well as with the isoalloxazine FAD ring. MD simulations showed that compound **22** formed stable H-bonds with FAD, whereas compounds **24** and **44** were involved in H-bonds with Tyr298 and Asn181, respectively. The potent MAO-A inhibitory activity of **22** compared with **24**,

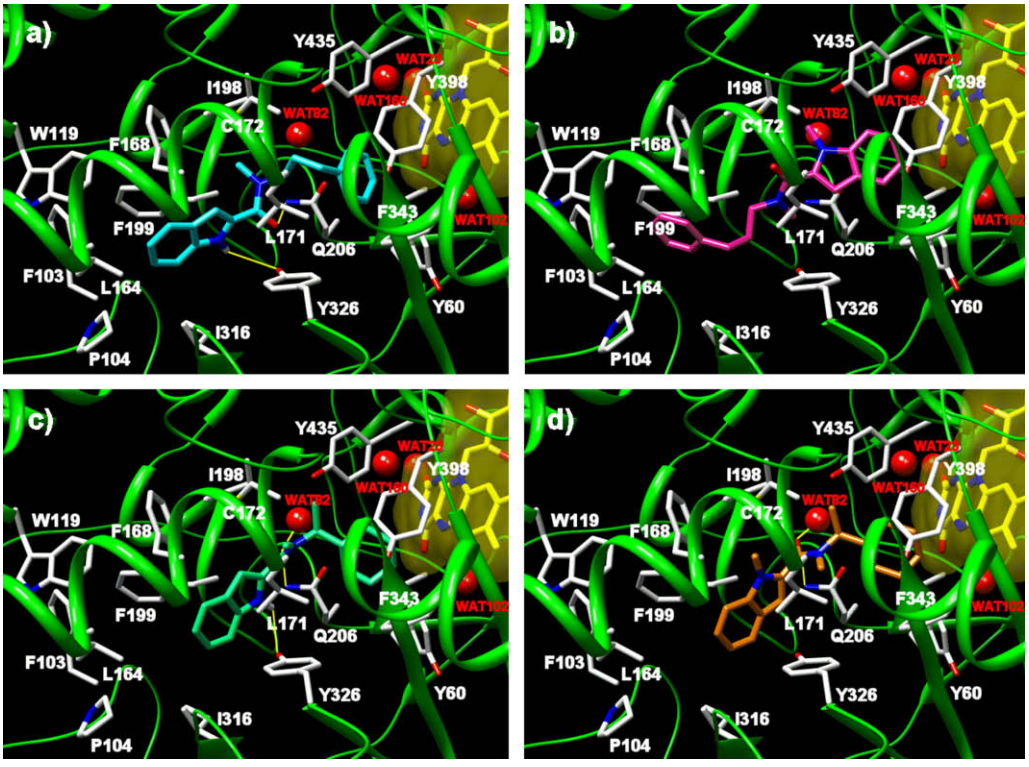

Figure 3. Binding modes of compounds **22** (cyan, a), **24** (magenta, b), **44** (spring green, c) and **46** (orange, d) into the mutated MAO-B binding cavity. For clarity, only interacting residues are displayed. Ligands, FAD cofactor (yellow) and interacting key residues (white) are represented as stick models, while the enzyme (green) as ribbons. Structural water molecules are represented as red balls. The van der Waals volume of FAD is displayed as a transparent yellow surface. H-bonds are shown as yellow lines.

44, and **46** was then regulated by its ability to establish close and productive interactions with FAD. Compounds **22**, **24**, **44**, and **46** fitted into the MAO-B active site with two prevailing binding modes. For **22**, **44**, and **46** the indole nucleus was hosted in the entrance cavity made up by lipophilic residues, whereas the phenyl or cyclohexyl rings occupied the substrate cavity which is directly in contact with the isoalloxazine FAD ring. Compound **22** was highly unstable during the MD simulation into the MAO-B, thus accounting for its low MAO-B affinity.

4. Experimental

4.1. Chemistry

4.1.1. Materials and methods

Melting points (mp) were determined on a Büchi 510 apparatus and are uncorrected. Infrared spectra (IR) were acquired with Perkin-Elmer 1310 and SpectrumOne spectrophotometers. Band position and absorption ranges are given in cm^{-1}. Proton nuclear magnetic resonance (^1H NMR) spectra were recorded on Bruker AM-200 (200 MHz) and Bruker Avance 400 MHz FT spectrometers in the indicated solvent. Chemical shifts are expressed in δ units (ppm) from tetramethylsilane. Column chromatographies were carried out with alumina (Merck, 70–230 mesh) and silica gel (Merck, 70–230 mesh). Aluminum oxide TLC cards (Fluka, aluminum oxide precoated aluminum cards with fluorescent indicator at 254 nm) and silica gel TLC cards (Fluka, silica gel precoated aluminum cards with fluorescent indicator at 254 nm) were used for thinlayer chromatography (TLC). Developed plates were visualized with a Spectroline ENF 260C/F UV apparatus. Organic solutions were dried over anhydrous sodium sulfate. Evaporation of the solvents was carried out on Büchi Rotavapor R-210 equipped with Büchi V-850 vacuum controller and Büchi V-700 (~5 mbar) and V-710 (~2 mbar) vacuum pumps. Elemental analyses of compounds 11–50 were found within ±0.4% of the theoretical values (Table 1S in Supplementary data).

4.1.2. General procedure for the synthesis of compounds 11–13, 15, 16, 18, 19, 21–23, 25, 26, 41, and 43–46. Example: *N*-Phenyl-1*H*-indole-2-carboxamide (11)

BOP reagent (8.22 g, 0.0186 mol) was added to a mixture of indole-2-carboxylic acid (3.00 g, 0.0186 mol), aniline (3.46 g, 3.38 mL, 0.0372 mol) and triethylamine (5.64 g, 7.77 mL, 0.056 mol) in anhydrous DMF (20 mL). The reaction mixture was stirred at 25 °C for 4 h, diluted with water and extracted with ethyl acetate. The organic layer was washed with 1 N HCl, brine and dried. Evaporation of the solvent furnished **11** (4.02 g, 91%), mp 190–192 °C (from ethanol). Lit.[26] 192–193 °C.

4.1.3. *N*-Methyl,*N*-phenyl-1*H*-indole-2-carboxamide (12)

Prepared as **11** using *N*-methylaniline. Yield 65%, mp 175–177 °C (from ethanol). Lit.[27] 173 °C.

4.1.4. *N*-Phenyl-1-methyl-1*H*-indole-2-carboxamide (13)

Prepared as **11** using 1-methyl-1*H*-indole-2-carboxylic acid and aniline. Yield 61%, mp 149–151 °C (from ethanol). Lit.[27] 147 °C.

4.1.5. *N*-Benzyl-1*H*-indole-2-carboxamide (15)

Prepared as **11** using benzylamine. Yield 88%, mp 222–224 °C (from ethanol). Lit.[28] 220 °C.

4.1.6. *N*-Benzyl,*N*-methyl-1*H*-indole-2-carboxamide (16)

Prepared as **11** using *N*-methylbenzylamine. Yield 70%, mp 195–198 °C (from ethanol). The quoted ^1H NMR spectral data was in agreement with values reported in Lit.[29]

4.1.7. *N*-(2-Phenylethyl)-1*H*-indole-2-carboxamide (18)

Prepared as **11** using 2-phenylethylamine. Yield 77%, mp 188–190 °C (from ethanol). ^1H NMR (DMSO-d_6): δ 2.85 (t, J = 7.6 Hz, 2 H), 3.48–3.53 (m, 2H), 6.99–7.03 (m, 1H), 7.06–7.07 (m, 1H), 7.13–7.20 (m, 2H), 7.23–7.30 (m, 4H), 7.39–7.41 (dd, J = 0.82 and 7.1 Hz, 1H), 7.58 (d, J = 8.0 Hz, 1H), 8.56 (br s, disappeared on treatment with D_2O, 1H), 11.53 ppm (br s, disappeared on treatment with D_2O, 1H). IR: ν 1630, 3257 cm^{-1}.

4.1.8. *N*-Methyl,*N*-(2-phenylethyl)-1*H*-indole-2-carboxamide (19)

Prepared as **11** (RS 2450) using *N*-methyl-*N*-(2-phenylethyl)amine. Yield 66%, mp 125–128 °C (from ethanol). ^1H NMR ($CDCl_3$): δ 3.04 (s, 2H), 3.30 (s, 3H), 3.89 (s, 2H), 6.82 (s, 1H), 7.12–7.16 (m, 1H), 7.24–7.35 (m, 6H), 7.45 (d, J = 8.0 Hz, 1H), 7.66 (d, J = 8.0 Hz, 1H), 9.82 ppm (br s, disappeared on treatment with D_2O, 1H). IR: ν 1596, 3247 cm^{-1}.

4.1.9. *N*-(3-Phenylpropyl)-1*H*-indole-2-carboxamide (21)

Prepared as **11** using 3-phenylpropylamine. Yield 76%, mp 176–178 °C (from ethanol). ^1H NMR (DMSO-d_6): δ *1.83–1.86* (m, 2H), 2.62–2.66 (m, 2H), 3.28–3.33 (m, 2H), 7.02 (t, J = 7.3 Hz, 1H), 7.11 (d, J = 2.0 Hz, 1H), 7.14–7.19 (m, 2H), 7.22–7.30 (m, 4H), 7.42 (d, J = 8.2 Hz, 1H), 7.59 (d, J = 8.0 Hz, 1H), 8.49 (t, J = 5.6 Hz, disappeared on treatment with D_2O, 1H), 11.55 ppm (br s, disappeared on treatment with D_2O, 1H). IR: ν 1619, 3289 cm^{-1}.

4.1.10. *N*-Methyl,*N*-(3-phenylpropyl)-1*H*-indole-2-carboxamide (22)

Prepared as **11** using **59**. Yield 84%, mp 147–150 °C (from ethanol). ^1H NMR ($CDCl_3$): δ 2.06 (s, 2H), 2.41–2.75 (m, 3H), 3.19–3.39 (m, 2H), 3.71 (s, 2H), 7.11–7.63 (m, 10H), 9.74 ppm (br s, disappeared on treatment with D_2O, 1H). IR: ν 1619, 3289 cm^{-1}.

4.1.11. *N*-(3-Phenylpropyl)-1-methyl-1*H*-indole-2-carboxamide (23)

Prepared as **11** using 1-methyl-1*H*-indole-2-carboxylic acid and 3-phenylpropylamine. Yield 75%, mp 80–84 °C (from ethanol). ^1H NMR (DMSO-d_6): δ 1.83–1.87 (m, 2H), 2.65 (t, J = 7.7 Hz, 2H), 3.26–3.31 (m, 2H), 3.97 (s, 3H), 7.07–7.31 (m, 8H), 7.51 (d, J = 8.1 Hz, 1H), 7.62 (d, J = 7.8 Hz, 1H), 8.52 ppm (br s, disappeared on treatment with D_2O, 1H). IR: ν 1624, 3297 cm^{-1}.

4.1.12. *N*-(4-Phenylbutyl)-1*H*-indole-2-carboxamide (25)

Prepared as **11** using 4-phenylbutylamine. Yield 85%, mp 119–121 °C (from ethanol). ^1H NMR (DMSO-d_6): δ 1.43–1.61 (m, 5H), 2.49–2.66 (m, 3H), 7.00 (t, J = 7.5 Hz, 1H), 7.14–7.19 (m, 5H), 7.23–7.27 (m, 2H), 7.40 (d, J = 8.4 Hz, 1H), 7.57 (d, J = 8.0 Hz, 1H), 8.45 (br s, disappeared on treatment with D_2O, 1H), 11.52 ppm (br s, disappeared on treatment with D_2O, 1H). IR: ν 1626, 3272 cm^{-1}.

4.1.13. *N*-Methyl,*N*-(4-phenylbutyl)-1*H*-indole-2-carboxamide (26)

Prepared as **11** using **60**. Yield 62% mp 131–133 °C (from ethanol). ^1H NMR (DMSO-d_6): δ 1.58–1.62 (m, 4H), 2.60 (s, 3H), 3.27–3.56 (m, 4H), 6.81–6.90 (m, 1H), 7.03 (t, J = 7.5 Hz, 1 H), 7.14–7.19 (m, 5H), 7.25 (t, J = 7.4 Hz, 1H), 7.42 (d, J = 8.3 Hz, 1H), 7.60 (d, J = 7.9 Hz, 1H), 11.53 ppm (br s, disappeared on treatment with D_2O, 1H). IR: ν 1599, 3260 cm^{-1}.

4.1.14. *(R,S)*-*N*-(α-Phenylethyl)-1*H*-indole-2-carboxamide (41)

Prepared as **11** using (*R,S*)-α-phenylethylamine. Yield 50%, mp 176–178 °C (ethanol). ^1H NMR (DMSO-d_6): δ 1.65 (d, J = 7.0 Hz, 3H), 5.32–5.39 (m, 1H), 7.17 (t, J = 7.5 Hz, 1H), 7.32 (t, J = 8.1 Hz, 1H), 7.37 (t, J = 7.2 Hz, 1H), 7.41 (s, 1H), 7.47 (t, J = 7.6 Hz, 2H), 7.55–7.58 (m, 3H), 7.76 (d, J = 8.0 Hz, 1H), 8.94 (br s, disappeared

on treatment with D_2O, 1H), 11.68 ppm (br s, disappeared on treatment with D_2O, 1H). IR: ν 1645, 3252, 3410 cm^{-1}.

4.1.15. (*R*)-*N*-(α-Cyclohexylethyl),*N*-methyl-1*H*-indole-2-carboxamide (43)

It was prepared as **11** using **61** Yield 60%, mp 150–154 °C (from ethanol). ^1H NMR ($CDCl_3$): δ 0.94–1.19 (m, 6H), 1.28–1.42 (m, 2H), 1.48–1.71 (m, 6H), 2.86 (s, 1H), 3.16 (s, 2H), 4.51–4.52 (m, 1H), 6.79 (s, 1H), 7.04 (t, J = 7.4 Hz, 1H), 7.19 (t, J = 7.8 Hz, 1H), 7.34 (d, J = 8.3 Hz, 1H), 7.57 (d, J = 8.0 Hz, 1H), 9.29 ppm (br s, disappeared on treatment with D_2O, 1H). IR: ν 1590, 3249 cm^{-1}.

4.1.16. (*S*)-*N*-(α-Cyclohexylethyl),*N*-methyl-1*H*-indole-2-carboxamide (44)

Prepared as **11** using **62**. Yield 42%, mp 160–163 °C (from ethanol). ^1H NMR ($CDCl_3$): δ 0.86–1.39 (m, 6H), 1.40–1.49 (m, 2H), 1.63–1.71 (m, 6H), 2.96 (s, 1H), 3.24 (s, 2H), 4.42–4.67 (m, 1H), 6.61 (s, 1H), 7.01 (t, J = 7.5 Hz, 1H), 7.15 (t, J = 7.5 Hz, 1H), 7.40 (d, J = 8.3 Hz, 1H), 7.58 (d, J = 7.9 Hz, 1H), 9.74 ppm (br s, disappeared on treatment with D_2O, 1H). IR: ν 1590, 3249 cm^{-1}.

4.1.17. (*R*)-*N*-(α-Cyclohexylethyl)-*N*-methyl-1-methyl-1*H*-indole-2-carboxamide (45)

Prepared as **11** using 1-methyl-1*H*-indole-2-carboxylic acid and **61**. Yield 59%, oil. ^1H NMR ($CDCl_3$): δ 0.67–0.73 (m, 1H), 1.02–1.31 (m, 7H), 1.42–1.82 (m, 6H), 2.97 (s, 3H), 3.83 (s, 3H), 3.96–4.54 (m, 1H), 6.53–6.62 (m, 1H), 7.16–7.19 (m, 1H), 7.28–7.33 (m, 1H), 7.38–7.41 (m, 1H), 7.65–7.67 ppm (m, 1H). IR: ν 1621 cm^{-1}.

4.1.18. (*S*)-*N*-(α-Cyclohexylethyl)-*N*-methyl-1-methyl-1*H*-indole-2-carboxamide (46)

Prepared as **11** using 1-methyl-1*H*-indole-2-carboxylic acid and **62**. Yield 59%, oil. ^1H NMR ($CDCl_3$): δ 0.64–0.71 (m, 1H), 0.99–1.27 (m, 7H), 1.45–1.82 (m, 6H), 2.94 (s, 3H), 3.80 (s, 3H), 3.93–4.52 (m, 1H), 6.51–6.59 (m, 1H), 7.13–7.16 (m, 1H), 7.26–7.28 (m, 1H), 7.36–7.38 (m, 1H), 7.62–7.64 ppm (m, 1H). IR: ν 1622 cm^{-1}.

4.1.19. General procedure for the synthesis of compounds 14, 17, 20, 24. Example. *N*-Methyl, *N*-phenyl-1-methyl-1*H*-indole-2-carboxamide (14)

Iodomethane (1.68 g, 0.74 mL, 0.012 mol) was added to an ice-cooled mixture of **12** (0.32 g, 0.002 mol), tetrabutylammonium hydrogen sulfate (0.68 g, 0.002 mol), dichlorometane (10 mL), and 50% NaOH solution (6.66 mL). The reaction was stirred at 25 °C for 3 h. Water was added while stirring and the mixture extracted with dichlorometane. The organic layer was separated, washed with brine, and dried to furnish **11** (0.76 g, 58%), mp 80–82 °C (from ethanol). Lit.[27] 84 °C.

4.1.20. *N*-Benzyl,*N*-methyl-1-methyl-1*H*-indole-2-carboxamide (17)

Prepared as **14** using **16**. Yield 90%, oil. ^1H NMR ($CDCl_3$): δ 3.12 (s, 3H), 3.90 (s, 3H), 4.84 (s, 2H), 6.67 (s, 1H), 7.14 (t, J = 7.3 Hz, 1H), 7.25–7.42 (m, 7H), 7.60 ppm (s, 1H). IR: ν 1625 cm^{-1}.

4.1.21. *N*-Methyl,*N*-(2-phenylethyl)-1-methyl-1*H*-indole-2-carboxamide (20)

Prepared as **14** using **19**. Yield 44%, mp 94–96 °C (from ethanol). ^1H NMR ($CDCl_3$): δ 2.92–3.09 (m, 5H), 3.55–3.76 (m, 3H), 3.85 (t, J = 7.1 Hz, 2H), 6.52 (s, 1H), 7.02–7.34 (m, 8H), 7.61 (d, J = 7.9 Hz, 1H). IR: ν 1619 cm^{-1}.

4.1.22. *N*-Methyl,*N*-(3-phenylpropyl)-1-methyl-1*H*-indole-2-carboxamide (24)

Prepared as **14** using **22**. Yield 97%, oil. ^1H NMR ($CDCl_3$): δ 2.04 (m, 2H), 2.55–2.73 (m, 2H), 3.16 (s, 3H), 3.67 (s, 2H), 3.84 (s, 3H), 6.60 (s, 1H), 7.15–7.38 (m, 8H), 7.62 ppm (d, J = 7.9 Hz, 1H). IR: ν 1624 cm^{-1}.

4.1.23. *N*-Methyl,*N*-(4-phenylbutyl)-1-methyl-1*H*-indole-2-carboxamide (27)

Iodomethane (4.25 g, 1.9 mL, 0.03 mol) was added to an ice-cooled mixture of **22** (1.50 g, 0.005 mol), tetrabutylammonium hydrogen sulfate (1.7 g, 0.005 mol), dichlorometane (25 mL) and 50% NaOH solution (16.6 mL). After stirring at 25 °C for 24 h, iodomethane (4.25 g, 1.9 mL, 0.03 mol) was added and the reaction mixture was stirred for additional 24 h. Water was added while stirring and the mixture extracted with chloroform. The organic layer was separated, washed with brine and dried. Removal of the solvent gave a residue which was purified by silica gel column chromatography (ethyl acetate/*n*-hexane = 3:1 as eluent) to furnish **27** (1.10 g, 69%) as an oil. ^1H NMR ($CDCl_3$): δ 1.55–1.73 (m, 4H), 2.61–2.72 (m, 2H), 3.13 (s, 3H), 3.59–3.62 (m, 2H), 3.82 (s, 3H), 6.60 (s, 1H), 7.13–7.23 (m, 4H), 7.30–7.36 (m, 3H), 7.39 (d, J = 7.0 Hz, 1H), 7.64 ppm (d, J = 7.9 Hz, 1H). IR: ν 1623 cm^{-1}.

4.1.24. General Procedure for the Synthesis of Compounds 28–31, 33, 34, 36–40, 42, and 47–50. Example. *N*-(1*H*-Indol-2-ylmethyl)-*N*-phenylamine (28)

A solution of **11** (2.00 g, 0.008 mol) in anhydrous THF (30 mL) was added dropwise to an ice-cooled suspension of $LiAlH_4$ (1.14 g, 0.03 mol) in the same solvent (38 mL). The reaction mixture was refluxed overnight. After cooling on an ice-bath the mixture was made basic with 10% NaOH solution and extracted with ethyl acetate. The organic layer was washed with brine and dried. Evaporation of the solvent furnished pure **28** (1.76 g, 99%). Mp 59–62 °C (from cyclohexane). ^1H NMR (DMSO-d_6): δ 4.36 (s, 2H), 6.05 (br s, disappeared on treatment with D_2O, 1H), 6.31 (s, 1H), 6.53 (t, J = 7.2 Hz, 1H), 6.65 (d, J = 7.8 Hz, 2H), 6.92 (t, J = 7.4 Hz, 1H), 6.98–7.07 (m, 3H), 7.30 (d, J = 8.1 Hz, 1H), 7.41 (d, J = 7.8 Hz, 1H), 11.00 ppm (br s, disappeared on treatment with D_2O, 1H). IR: ν 3054, 3402 cm^{-1}.

4.1.25. *N*-(1*H*-Indol-2-ylmethyl)-*N*-methyl-*N*-phenylamine (29)

Prepared as **28** using **12**. Yield 74%, oil. ^1H NMR (DMSO-d_6): δ 3.03 (s, 3H), 4.65 (s, 2H), 6.20 (s, 1H), 6.52–6.55 (m, 1H), 6.65 (t, J = 7.6 Hz, 1H), 6.83 (d, J = 8.1 Hz, 1H), 6.94 (t, J = 7.8 Hz, 1H), 7.03 (t, J = 7.8 Hz, 1H), 7.17 (t, J = 8.0 Hz, 2H), 7.33 (d, J = 8.0 Hz, 1H), 7.42 (d, J = 7.4 Hz, 1H), 10.99 ppm (br s, disappeared on treatment with D_2O, 1H). IR: ν 3399 cm^{-1}.

4.1.26. *N*-(1-Methyl-1*H*-indol-2-ylmethyl)-*N*-phenylamine (30)

Prepared as **28** using **13**. Yield 43%, mp 76–78 °C (ethanol). ^1H NMR (DMSO-d_6): δ 3.75 (s, 3H), 4.43 (d, J = 5.5 Hz, 2H), 6.08 (br s, disappeared on treatment with D_2O, 1H) 6.41 (s, 1H), 6.54–6.58 (m, 1H), 6.72 (d, J = 6.8 Hz, 2H), 7.00 (t, J = 7.5 Hz, 1H), 7.03–7.13 (m, 3H), 7.41 (d, J = 8.2 Hz, 1H), 7.48 ppm (br s, disappeared on treatment with D_2O, 1H). IR: ν 3399 cm^{-1}.

4.1.27. *N*-(1-Methyl-1*H*-indol-2-ylmethyl)-*N*-methyl-*N*-phenylamine (31)

Prepared as **28** using **14**. Yield 62%, mp 131–136 °C (*n*-hexane). ^1H NMR ($CDCl_3$): δ 2.91 (s, 3 H), 3.70 (s, 3H), 4.59 (s, 2H), 6.39 (s, 1H), 6.80 (t, J = 7.2 Hz, 1H), 6.90 (d, J = 8.3 Hz, 2H), 7.10 (t, J = 7.5 Hz, 1H), 7.19 (t, J = 6.7 Hz, 1H), 7.25–7.32 (m, 3H), 7.55 (d, J = 7.8 Hz, 1H).

4.1.28. *N*-Benzyl-*N*-(1*H*-indol-2-ylmethyl)-*N*-methylamine (33)

Prepared as **28** using **16**. Yield 45%, oil. ^1H NMR ($CDCl_3$): δ 2.25 (s, 3H), 3.61 (s, 2H), 3.74 (s, 2H), 6.39 (s, 1H), 7.09 (t, J = 8.0 Hz, 1H), 7.2 (t, J = 8.0 Hz, 1H), 7.25–7.32 (m, 1H), 7.34–7.38 (m, 5H), 7.57 (d,

J = 7.8 Hz, 1H), 8.69 ppm (br s, disappeared on treatment with D_2O, 1H). IR: ν 3130 cm^{-1}.

4.1.29. *N*-Benzyl-*N*-(1-methyl-1*H*-indol-2-ylmethyl)-*N*-methylamine (34)

Prepared as **28** using **17**. Yield 85%, oil. ^1H NMR ($CDCl_3$): δ 2.23 (s, 3H), 3.60 (s, 2H), 3.71 (s, 2H), 3.83 (s, 3H), 6.46 (s, 1H), 7.13 (t, J = 7.4 Hz, 1H), 7.2 (t, J = 8.2 Hz, 1H), 7.35–7.38 (m, 6H), 7.62 ppm (d, J = 7.9 Hz, 1H).

4.1.30. *N*-(1*H*-Indol-2-ylmethyl)-*N*-methyl-*N*-(2-phenethyl)amine (36)

Prepared as **28** using **19**. Yield 45%, oil. ^1H NMR ($CDCl_3$): δ 2.36 (s, 3H), 2.67 (t, J = 7.2 Hz, 2 H), 2.81 (t, J = 7.1 Hz, 2H), 3.70 (s, 2H), 6.29 (s, 1H), 7.05–7.20 (m, 5H), 7.26–7.32 (m, 3H), 7.51 (d, J = 7.7 Hz, 1H), 8.1 ppm (br s, disappeared on treatment with D_2O, 1H). IR: ν 3412 cm^{-1}.

4.1.31. *N*-(1-Methyl-1*H*-indol-2-ylmethyl)-*N*-methyl-*N*-(2-phenethyl)amine (37)

Prepared as **28** using **20**. Yield 68%, oil. ^1H NMR ($CDCl_3$): δ 2.31 (s, 3H), 2.73 (t, J = 7.8 Hz, 2H), 2.83 (t, J = 7.2 Hz, 2H), 3.62 (s, 3H), 3.67 (s, 2H), 6.39 (s, 1H), 7.10 (t, J = 7.8 Hz, 1H), 7.16 (d, J = 8.5 Hz, 2H), 7.20–7.23 (m, 3H), 7.25–7.31 (m, 2H), 7.59 ppm (d, J = 7.3 Hz, 1H).

4.1.32. *N*-(1*H*-Indol-2-ylmethyl)-*N*-methyl-*N*-(2-phenylpropyl)amine (38)

Prepared as **28** using **22**. Yield 52%, oil. ^1H NMR ($CDCl_3$): δ 1.84–1.92 (m, 2H), 2.25 (s, 3H), 2.50 (t, J = 7.4 Hz, 2H), 2.67 (t, J = 7.7 Hz, 2H), 3.68 (s, 2H), 6.36 (s, 1H), 7.11 (t, J = 7.9 Hz, 1H), 7.16–7.24 (m, 4H), 7.29–7.36 (m, 3H), 7.58 (d, J = 7.8 Hz, 1H), 8.65 ppm (br s, disappeared on treatment with D_2O, 1H). IR: ν 3414 cm^{-1}.

4.1.33. *N*-(1-Methyl-1*H*-indol-2-ylmethyl)-*N*-methyl-*N*-(2-phenylpropyl)amine (39)

Prepared as **28** using **24**. Yield 74%, oil. ^1H NMR ($CDCl_3$): δ 1.81–1.89 (m, 2H), 2.24 (s, 3H), 2.47 (t, J = 7.1 Hz, 2H), 2.64 (t, J = 7.8 Hz, 2H), 3.64 (s, 2H), 3.84 (s, 3H), 6.37 (s, 1H), 7.09–7.26 (m, 4H), 7.22–7.35 (m, 3H), 7.33 (d, J = 8.2 Hz, 1H), 7.59 ppm (d, J = 7.8, 1H).

4.1.34. *N*-(1*H*-Indol-2-ylmethyl)-*N*-(4-phenylbutyl)amine (40)

Prepared as **28** using **25**. Yield 47%, oil. ^1H NMR ($CDCl_3$): δ 1.48–1.54 (m, 2H), 1.56–1.62 (m, 2H), 2.54 (t, J = 7.5 Hz, 2H), 2.63 (t, J = 7.1 Hz, 2H), 3.93 (s, 2H), 6.32 (s, 1H), 6.95 (t, J = 7.4 Hz, 1H), 7.04 (t, J = 7.5 Hz, 1H), 7.14–7.18 (m, 3H), 7.24–7.28 (m, 2H), 7.33 (d, J = 7.9 Hz, 1H), 7.45 (d, J = 7.8 Hz, 1H), 8.33 (br s, disappeared on treatment with D_2O, 1H), 11.07 ppm (br s, disappeared on treatment with D_2O, 1H). IR: ν 3414 cm^{-1}.

4.1.35. (*R*,*S*)-*N*-(1*H*-Indol-2-ylmethyl)-*N*-(α-phenylethyl)amine (42)

Prepared as **28** using **41**. Yield 47%, oil. ^1H NMR (DMSO-d_6): δ 1.27 (d, J = 6.6 Hz, 3H), 3.35 (br s, disappeared on treatment with D_2O, 1H), 3.57–3.73, (m, 2H), 3.71 (q, J = 6.6 Hz, 1H), 6.18 (s, 1H), 6.89–6.93 (m, 1H), 6.97–7.01 (m, 1H), 7.22–7.24 (m, 1H), 7.29–7.37 (m, 5H), 7.40 (d, J = 7.7 Hz, 1H), 10.86 ppm (br s, disappeared on treatment with D_2O, 1H). IR: ν 3410, 3415 cm^{-1}.

4.1.36. (*R*)-*N*-(α-Cyclohexylethyl)-*N*-(1*H*-indol-2-ylmethyl)amine (47)

Prepared as **28** using **43**. Yield 96%, oil. ^1H NMR ($CDCl_3$): δ 0.83–0.96 (m, 5H), 1.15–1.44 (m, 4H), 1.66–1.81 (m, 4H), 2.13 (s, 3H), 2.18–2.21 (m, 1H), 2.32–2.39 (m, 1H), 3.65 (d, J = 14.1 Hz, 1H), 3.77 (d, J = 14.1 Hz, 1H), 6.31 (s, 1H), 7.07 (t, J = 7.1 Hz, 1H), 7.12 (t, J = 7.9 Hz, 1H), 7.35 (d, J = 7.1 Hz, 1H), 7.53 (d, J = 7.8 Hz, 1H), 8.47 ppm (br s, disappeared on treatment with D_2O, 1H). IR: ν 3458 cm^{-1}.

4.1.37. (*S*)-*N*-(α-Cyclohexylethyl)-*N*-(1*H*-indol-2-ylmethyl)amine (48)

Prepared as **28** using **44**. Yield 91%, oil. ^1H NMR ($CDCl_3$): δ 0.83–0.94 (m, 5H), 1.11–1.44 (m, 4H), 1.66–1.80 (m, 4H), 2.13 (s, 3H), 2.18–2.22 (m, 1H), 2.33–2.37 (m, 1H), 3.65 (d, J = 14.3 Hz, 1H), 3.76 (d, J = 14.2 Hz, 1H), 6.31 (s, 1 H), 7.08 (t, J = 7.2 Hz, 1H), 7.14 (t, J = 8.0 Hz, 1H), 7.34 (d, J = 7.1 Hz, 1H), 7.53 (d, J = 7.8 Hz, 1H), 8.47 ppm (br s, disappeared on treatment with D_2O, 1H). IR: ν 3458 cm^{-1}.

4.1.38. (*R*)-*N*-(α-Cyclohexylethyl)-*N*-(1*H*-indol-2-ylmethyl)-*N*-methylamine (49)

Prepared as **28** using **45**. Yield 89%, oil. ^1H NMR ($CDCl_3$): δ 0.71–0.78 (m, 2H), 0.90–0.93 (m, 3H), 1.04–1.36 (m, 5H), 1.56–1.71 (m, 4H), 2.03 (s, 3H), 2.31–2.37 (m, 1H), 3.63–3.65 (m, 2H), 3.74 (s, 3H), 6.31 (s, 1H), 6.98 (t, J = 7.4 Hz, 1H), 7.09 (t, J = 7.6 Hz, 1H), 7.38 (d, J = 8.2 Hz, 1H), 7.46 ppm (d, J = 7.8 Hz, 1H).

4.1.39. (*S*)-*N*-(α-Cyclohexylethyl)-*N*-(1*H*-indol-2-ylmethyl)-*N*-methylamine (50)

Prepared as **28** using **46**. Yield 78%, oil. ^1H NMR ($CDCl_3$): δ 0.70–0.75 (m, 2H), 0.93–0.95 (m, 3H), 1.10–1.31 (m, 5H), 1.61–1.74 (m, 4H), 2.06 (s, 3H), 2.33–2.37 (m, 1H), 3.64–3.73 (m, 2H), 3.78 (s, 3H), 6.33 (s, 1H), 7.08 (t, J = 8.1 Hz, 1H), 7.18 (t, J = 8.1 Hz, 1H), 7.29 (d, J = 74 Hz, 1H), 7.56 ppm (d, J = 7.8 Hz, 1H).

4.1.40. General procedure for the synthesis of compounds 55–60. Example: ethyl *N*-(3-phenylpropyl)carbamate (55)

Ethyl chloroformate (0.78 g, 0.67 mL, 0.0072 mol) in anhydrous THF (15 mL) was added to a solution of 3-phenylpropylamine (0.98 g, 1.04 mL, 0.0072 mol) and triethylamine (0.73 g, 1.00 mL, 0.0072 mol) in the same solvent (38 mL). The reaction mixture was stirred at 25 °C for 2 h. Water and ethyl acetate were added and the organic layer was separated, washed with brine, and dried. Evaporation of the solvent furnished pure **55** (1.42 g, 95%) as an oil. The quoted ^1H NMR spectral data was in agreement with values reported in Lit.[30]

4.1.41. Ethyl *N*-(3-phenylbutyl)carbamate (56)

Prepared as **55** using 4-phenylbutylamine. Yield 96%, oil. ^1H NMR: δ 1.24 (t, J = 7.1 Hz, 3H), 1.49–1.54 (m, 2H), 1.61–1.68 (m, 2H), 2.63 (t, J = 7.4, 2H), 3.18 (q, J = 6.5 Hz, 2H), 4.11 (q, J = 7.1 Hz, 2H), 4.61 (br s, disappeared on treatment with D_2O, 1H), 7.15–7.20 (m, 3H), 7.25–7.29 ppm (m, 2H). IR: ν 1710, 2993, 3338 cm^{-1}.

4.1.42. Ethyl (*R*)-(α-cyclohexylethyl)carbamte (57)

Prepared as **55** using (*R*)-α-cyclohexylethylamine. Yield 89%, mp 46–48 °C (from cyclohexane). Lit.[31] 49–50 °C.

4.1.43. 4.1.43.Ethyl (*S*)-(α-cyclohexylethyl)carbamate (58)

Prepared as **55** using (*S*)-α-cyclohexylethylamine. Yield 89%, mp 46–48 °C (from cyclohexane). Lit.[31] 49–50 °C.

4.1.44. *N*-(3-Phenylpropyl)-*N*-methylamine (59)

Prepared as **28** using **55**. Yield 84%, oil. The quoted ^1H NMR spectral data was in agreement with values reported in Lit.[32]

4.1.45. *N*-(3-Phenylbutyl)-*N*-methylamine (60)

Prepared as **28** using **56**. Yield 81%, oil. The quoted ^1H NMR spectral data was in agreement with values reported in Lit.[33]

4.1.46. (*R*)-*N*-(α-Cyclohexylethyl)-*N*-methylamine (61)

Prepared as **28** using **57**. Yield 59%, oil. The quoted ^{1}H NMR spectral data was in agreement with values reported in Lit.[34]

4.1.47. (*S*)-*N*-(α-Cyclohexylethyl)-*N*-methylamine (62)

Prepared as **28** using **58**. Yield 58%, oil. The quoted ^{1}H NMR spectral data was in agreement with values reported in Lit.[35]

4.2. Biology

4.2.1. Mitochondria preparation

Mitochondria were prepared according to Basford.[13] Reagents: Medium A contained 0.4 M sucrose, 0.001 EDTA, 0.02% polyethersulfone (PES) or heparin and pH was adjusted to 6.8–7.0 with KOH; Medium F made was made up of the Medium A to which Ficoll was added to a final concentration of 8%. Calf or beef brains were removed from the animals within 5–10 min after their death. The brains were immediately placed in cold Medium A, stored on ice, and then transported to the laboratory. In a cold room, at 5 °C, the cerebral hemispheres were removed from the brains and the meninges were taken up with forceps. The gray matter was scraped from the cortices using a dull spatula. Two brains yield corresponded to about 100 g of wet tissue, which was homogenized in Medium A (2 mL/g of wet tissue). The homogenate was kept at pH 7.0 by adding some drops of Tris-buffer 2 M; 1 mg of ε-aminocaproic acid/g of tissue was added and then the mixture was stirred at 0–4 °C for 15 min. The suspension was diluted with Medium A (20 mL/g of the original tissue), centrifuged first at 184*g* for 20 min and then at 1153*g* for 20 min, without transferring of the supernatant. The residue R_1 was discarded while the supernatant S_1 was centrifuged at 12,000*g* for 15 min, to yield a crude mitochondria pellet R_2 (the supernatant S_2 which is discarded). The fraction R_2 was dissolved in Medium F (6 mL/g of original tissue), gently homogenized and centrifuged at 12,000*g* for additional 30 min. The resulting mitochondria fraction R_3 was washed using 4 mL of Medium A/g of original tissue and again centrifuged at 12,000*g* for 15 min. The final mitochondria fraction R_4, was homogenized in potassium phosphate buffer pH 7.4, 0.25 M. The yield of mitochondria protein obtained was between 100 and 140 mg per 50 g wet weight of the original tissue.

4.2.2. Activity assay

Monoamine oxidase activity was determined using kinuramine as a substrate, at four different final concentrations ranging from 5 μM to 0.1 mM, by a sensitive fluorometric assay according to Matsumoto et al.[14] In all assays the incubation mixtures contained: potassium phosphate buffer, pH 7.4, mitochondria (6 mg/mL), drug solutions in DMSO, added to the reaction mixture at a final concentration ranging from 0 to 10^{-9}. Solutions were preincubated for 30 min before adding the substrate and then incubated for others 30 min. The inhibitory activities against MAO-A and MAO-B were determined at 38 °C, after incubation of the mitochondrial fractions for 30 min in the presence of the specific inhibitor (L-deprenyl (1 μM) or clorgyline (1 μM) to estimate the MAO-A and MAO-B activity, respectively). The addition of percloric acid ended the reaction. Then the samples were centrifuged at 10,000*g* for 5 min and the supernatant was added to 2.7 mL NaOH 1N. Fluorometric measurements were recorded at $\lambda_{exc.}$ 317 nm and λ_{em} 393 nm using a Perkin-Elmer LS 50B spectrofluorometer. Dixon plot were used to estimate the inhibition constant (K_i) of the inhibitors. Data are the means of three or more experiments each performed in duplicate.

4.3. Molecular modeling

4.3.1. Computational chemistry

Molecular modeling and graphics manipulations were performed using Molecular Operating Environment (MOE)[36] and UCSF-CHIMERA[37] software packages, running on a Silicon Graphics Tezro R16000 workstation. Energy minimizations and MD simulations were realized by employing the AMBER 9 program,[38] selecting the parm99 force field.[39]

4.3.2. Ligand and protein setup

Model building and geometry optimizations of compounds **22, 24, 44**, and **46** were accomplished with the MMFF94X force field[40–44] available within MOE. The crystal structure of rat MAO-A (entry code: 1O5W)[15] and human MAO-B (entry code: 1OJC)[16,17] recovered from Brookhaven Protein Database[45] were used for the docking experiments. The choice of using 1OJC structure was guided by the quality of the crystallographic data and the fact that *N*-(2-aminoethyl)-*p*-chlorobenzamide was (at the time of the simulation) the only cocrystallized noncovalent ligand crossing the entire binding site of MAO-B. As a consequence, the side chain of key residue Ile199 is oriented such as the 'entrance' and 'substrate' cavities are fused. To simulate the active site of the bovine MAO-B, the 1OJC model, containing the four conserved water molecules (WAT23, WAT82, WAT102, and WAT160), was virtually mutated replacing the Ile199 with a Phe residue. The side chain of Phe199 was rotated into the 'open' conformation in such a way to allow for larger inhibitors to span both cavities, as Hubàlek and coworkers suggested.[46,47] Hydrogen atoms were added to both 1O5W and 1OJC in agreement with the ionization state existing at physiological pH. Partial atomic charges were computed by MOE using the Amber99 force field. Since the X-ray structures might contain residual energetic tensions from the crystallization process, both structures were subjected to a preliminary constrained energy minimization of those residues out of a radius of 15 Å from the N5 of the isoalloxazine ring in order to restore the natural planarity of the FAD ring and relax the active site amino acids. Subsequently, the resulting energy-minimized structures were deprived of the covalent ligands (clorgyline for 1O5W and *N*-(2-aminoethyl)-*p*-chlorobenzamide for 1OJC) and used as starting models for docking simulations.

4.3.3. Docking simulations

Docking of **22, 24, 44**, and **46** to both MAO-A and MAO-B was performed with GOLD 3.1,[19,20] which uses a genetic algorithm for determining the docking modes of ligands and proteins. An advantage of GOLD over other docking methods is the program's ability to account for some rotational protein flexibility, as well as full ligand flexibility. Specifically, OH groups of Ser, Thr, and Tyr, and amino groups of Lys are allowed to rotate during docking to optimize H-bonding to the ligand. GOLD requires a user-defined binding site. It searches for a cavity within the defined area, and considers all the solvent-accessible atoms in that area as active site atoms. On the basis of the GOLD score, for each molecule a bound conformation with high score was considered as the best bound conformation. The score function that was implemented in GOLD consisted basically of H-bonding, complex energy, and ligand internal energy terms. A population of possible docked orientations of the ligand is set up at random. Each member of the population is encoded as a 'chromosome', which contains information about the mapping of ligand H-bond atoms onto (complementary) protein H-bond atoms, mapping of hydrophobic points of the ligand onto protein hydrophobic points, and the conformation around flexible ligand bonds and protein OH groups. A number of parameters control the precise operation

of the genetic algorithm. Fifty independent docking runs were performed for each docking experiment, using standard default settings with a population size of 100, a maximum number of 100,000 operations, and a mutation and crossover rate of 95. The protein input file may be the entire protein structure or a part of it comprising only the residues that are in the region of the ligand binding site. In the present study, GOLD was allowed to calculate interaction energies within a sphere of a 13 Å radius centered on the phenolic oxygen atom of Tyr444 and Tyr435 in MAO-A and MAO-B, respectively. After docking, the 20 individual binding poses of each ligand were re-ranked according to the *GOLDscore* (details in the text). The top-ranked conformation of each ligand was selected and the corresponding *GOLDscore* was then correlated with the inhibition constant $pK_i(-\log K_i)$.

All the parameters were used as GOLD default values, and the ligands were submitted to 20 genetic algorithm runs. The program was set to allow early termination if the top 3 solutions are within 1.0 Å rmsd of each other, which we feel would indicate that the poses have reached an optimum based on the fitness function. The four water molecules detected in the MAO-B binding site were used in the docking studies. GOLD automatically determined whether they should be bound or displaced by toggling it on and off during the docking run, and, furthermore, the orientation of the water hydrogen atoms were optimized by GOLD during docking. After docking, the predicted binding poses of each ligand were re-ranked according to the *GOLDscore* (details in the text). Finally, the top-ranked conformation of each ligand was used for further studies.

4.3.4. Molecular dynamics simulations

All MD simulations were performed using the SANDER module in the AMBER suite of programs, employing the Cornell et al. force field[39] to assign parameters for the standard amino acids. General AMBER force field (GAFF) parameters were assigned to ligands, while the partial charges were calculated using the AM1-BCC method as implemented in the ANTECHAMBER suite of AMBER. The complexes were soaked in a box of TIP3P[48] water molecules with a margin of 10 Å along each dimension. An appropriate number of counterions were added to neutralize the system. The entire system was then minimized for 5000 steps using combined steepest descent and conjugate gradient methods until a convergence value of 0.001 kcal/mol Å. Upon minimization, harmonic constraints of 2 kcal/Å^2/mol on the protein backbone atoms of the complexes were applied. Such a energy minimization was designed to resolve the clashes between the complex and solvent molecules gradually. The complexes were then subjected to a two stage equilibration to further relax the protein and the surrounding solvent. In the first stage, the systems were heated from 0 to 300 K (using the Langevin dynamics method) over 50 ps of simulation time. We performed this stage of equilibration with the volume held constant. In the second stage, the systems were equilibrated for 50 ps using pressure and temperature control to adjust the density of water to experimental values. A subsequent production run was performed at a constant temperature of 300 K and a constant volume, giving a total simulation time of 500 ps. The time step of the simulations was 2.0 fs with a cut-off of 8 Å for the no bonded interaction, and SHAKE[49] was employed to keep all bonds involving hydrogen atoms rigid. Coordinates were saved every 1 ps and used to calculate the averaged structures from the simulations. The averaged structures over the last 300 ps of the simulations were energy-minimized as previously described and store as the final conformation of the ligand–enzyme complexes.

Acknowledgments

This work was partially supported by the Italian MIUR (Ministero dell'Istruzione, Università e Ricerca) and by funds MIUR-PRIN (Cofin) (EA).

Supplementary data

Supplementary data associated with this article can be found, in the online version, at doi:10.1016/j.bmc.2008.09.072.

References and notes

1. Mondovì, B. *Structure and Function of Amine Oxidases*; CRC Press: Boca Raton, FL, 1985.
2. (a) Abell, C. W.; Kwan, S.-W. *Prog. Nucl. Acid Res. Mol. Biol.* **2001**, *65*, 129–156; (b) Grimsby, J.; Lan, N. C.; Neve, R.; Chen, K.; Shih, J. C. *J. Neurochem.* **1990**, *55*, 1166–1169; (c) Tipton, K. F.; Boyce, S.; O'Sullivan, J.; Davey, G. P.; Healey, J. *Curr. Med. Chem.* **2004**, *11*, 1965–1982.
3. (a) Cesura, A. M.; Pletscher, A. *Prog. Drug Res.* **2002**, *38*, 171–298; (b) Yamada, M.; Yasuhara, H. *Neurotoxicology* **2004**, *25*, 215–221.
4. (a) Drukarch, B.; van Muiswinkel, F. L. *Biochem. Pharm.* **2000**, *59*, 1023–1031; (b) Schapira, A. H. V. *Arch. Neurol.* **2007**, *64*, 1083–1088.
5. Boyer, E. W.; Shannon, M. *N. Engl. J. Med.* **2005**, *352*, 1112–1120.
6. (a) Sagi, Y.; Drigues, N.; Youdim, M. B. H. *Br. J. Pharm.* **2005**, *146*, 553–560; (b) Youdim, M. Y. B.; Bakhle, Y. S. *Br. J. Pharm.* **2006**, *147*, S287–S296.
7. Avramovich-Tirosh, Y.; Amit, T.; Bar-Am, O.; Zheng, H.; Fridkin, M.; Youdim, M. B. H. *J. Neurochem.* **2007**, *100*, 490–502.
8. Silvestri, R.; La Regina, G.; De Martino, G.; Artico, M.; Befani, O.; Palumbo, M.; Agostinelli, E.; Turini, M. *J. Med. Chem.* **2003**, *46*, 917–920.
9. La Regina, G.; Silvestri, R.; Artico, M.; Lavecchia, A.; Novellino, E.; Befani, O.; Turini, P.; Agostinelli, E. *J. Med. Chem.* **2007**, *50*, 922–931.
10. Perez, V.; Unzeta, M. *Neochem. Int.* **2003**, *42*, 221–229.
11. Sanz, E.; Romera, M.; Belyk, L.; Marco, J. I.; Unzeta, M. *Med. Sci. Monitor* **2004**, *10*, BR477–BR484.
12. Morón, J. A.; Campillo, M.; Perez, V.; Unzeta, M.; Pardo, M. *J. Med. Chem.* **2000**, *43*, 1684–1691.
13. Basford, R. E. *Methods Enzymol.* **1967**, *10*, 96–101.
14. Matsumoto, T.; Suzuki, O.; Furuta, T.; Asai, M.; Kurokawa, Y.; Rimura, Y.; Katsumata, Y.; Takahashi, I. *Clin. Biochem.* **1985**, *18*, 126–129.
15. Ma, J.; Yoshimura, M.; Yamashita, E.; Nakagawa, A.; Ito, A.; Tsukihara, T. *J. Mol. Biol.* **2004**, *338*, 103–114.
16. Binda, C.; Newton-Vinson, P.; Hubalek, F.; Edmondson, D. E.; Mattevi, A. *Nat. Struct. Biol.* **2002**, *9*, 22–26.
17. Binda, C.; Li, M.; Hubalek, F.; Restelli, N.; Edmondson, D. E.; Mattevi, A. *Proc. Natl. Acad. Sci. U.S.A.* **2003**, *100*, 9750–9755.
18. Database searching (SWISS-PROT), sequence alignment, and analysis of rat, bovine and human MAO sequences were carried out using FASTA Pearson, W. R. *Proc. Natl. Acad. Sci. U.S.A.* **1988**, *85*, 2444–2448; and BLAST programs Wang, S.; Pak, Y. J. *Phys. Chem. B* **2000**, *104*, 354–359.
19. GOLD 3.1; CCDC Software Limited: Cambridge, UK, 2004.
20. Jones, G.; Willett, P.; Glen, R. C.; Leach, A. R.; Taylor, R. *J. Mol. Biol.* **1997**, *267*, 727–748.
21. Schulz-Gasch, T.; Stahl, M. *J. Mol. Model.* **2003**, *9*, 47–57.
22. Wang, R.; Lu, Y.; Wang, S. *J. Med. Chem.* **2003**, *46*, 2287–2303.
23. Kellenberger, E.; Rodrigo, J.; Muller, P.; Rognan, D. *Proteins: Struct. Funct. Bioinf.* **2004**, *57*, 225–242.
24. Warren, G. L.; Andrews, C. W.; Capelli, A. M.; Clarke, B.; LaLonde, J.; Lambert, M. H.; Lindvall, M.; Nevins, N.; Semus, S. F.; Senger, S.; Tedesco, G.; Wall, I. D.; Woolven, J. M.; Peishoff, C. E.; Head, M. S. *J. Med. Chem.* **2006**, *49*, 5912–5931.
25. Verdonk, M. L.; Cole, J. C.; Hartshorn, M. J.; Murray, C. W.; Taylor, R. D. *Proteins* **2003**, *52*, 609–623.
26. Mahboobi, S.; Teller, S.; Pongratz, H.; Hufsky, H.; Sellmer, A.; Botzki, A.; Uecker, A.; Beckers, T.; Baasner, S.; Schaechtele, C.; Ueberall, F.; Kassack, M. U.; Dove, S.; Boehmer, F. D. *J. Med. Chem.* **2002**, *45*, 1002–1018.
27. Caubere, C.; Caubere, P.; Renard, P.; Bizot-Espiart, J. G.; Ianelli, S.; Nardelli, M.; Jamart-Gregoire, J. *Tetrahedron* **1994**, *50*, 13433–13448.
28. Pigulla, J.; Roeder, E. *Arch. Pharm.* **1979**, *312*, 12–18.
29. Ellames, G. J.; Gibson, J. S.; Herbert, J. M.; McNeill, A. H. *Tetrahedron* **2001**, *57*, 9487–9497.
30. Inesi, A.; Mucciante, V.; Rossi, L. *J. Org. Chem.* **1998**, *63*, 1337–1338.
31. McGahren, W. J.; Kunstmann, M. P. *J. Org. Chem.* **1972**, *37*, 902–906.
32. Kuehne, M. E.; Shannon, P. J. *J. Org. Chem.* **1977**, *42*, 2082–2087.
33. Ding, C. Z.; Lu, X.; Nishimura, K.; Silverman, R. B. *J. Med. Chem.* **1993**, *36*, 1711–1715.
34. Willoughby, C. A.; Buchwald, S. L. *J. Am. Chem. Soc.* **1994**, *116*, 8952–8965.
35. Verdaguer, X.; Lange, U. E. W.; Reding, M. T.; Buchwald, S. L. *J. Am. Chem. Soc.* **1996**, *118*, 6784–6785.
36. Molecular Operating Environment (MOE), version 2005.06; Chemical Computing Group, Inc.: Montreal, Canada, 2005.

37. Huang, C. C.; Couch, G. S.; Pettersen, E. F.; Ferrin, T. E. *Pac. Symp. Biocomput.* **1996**, *1*, 724
38. Case, D. A.; Darden, T. A.; Cheatham, T. E., III; Simmerling, C. L.; Wang, J.; Duke, R. E.; Luo, R.; Merz, K. M.; Pearlman, D. A.; Crowley, M.; Walker, R. C.; Zhang, W.; Wang, B.; Hayik, S.; Roitberg, A.; Seabra, G.; Wong, K. F.; Paesani, F.; Wu, X.; Brozell, S.; Tsui, V.; Gohlke, H.; Yang, L.; Tan, C.; Mongan, J.; Hornak, V.; Cui, G.; Beroza, P.; Mathews, D. H.; Schafmeister, C.; Ross, W. S.; Kollman, P. *AAMBER 9*; University of California: San Francisco, 2006.
39. Cornell, W. D.; Cieplak, P.; Bayly, C. I.; Gould, I. R.; Merz, K. M., Jr.; Ferguson, D. M.; Spellmeyer, D. C.; Fox, T.; Caldwell, J. W.; Kollman, P. A. *J. Am. Chem. Soc.* **1995**, *117*, 5179–5197.
40. Halgren, T. A. *J. Comput. Chem.* **1996**, *17*, 490–512.
41. Halgren, T. A. *J. Comput. Chem.* **1996**, *17*, 520–552.
42. Halgren, T. A. *J. Comput. Chem.* **1996**, *17*, 553–586.
43. Halgren, T. A. *J. Comput. Chem.* **1996**, *17*, 587–615.
44. Halgren, T. A. *J. Comput. Chem.* **1996**, *17*, 616–641.
45. Bernstein, F. C.; Koetzle, T. F.; Williams, G. J. B.; Meyer, E. F., Jr.; Brice, M. D.; Rodgers, J. R.; Kennard, O.; Shimanouchi, T.; Tasumi, T. *J. Mol. Biol.* **1977**, *112*, 535–542.
46. Hubálek, F.; Binda, C.; Khalil, A.; Li, M.; Mattevi, A.; Castagnoli, N.; Edmondson, D. E. *J. Biol. Chem.* **2005**, *16*, 15761–15766.
47. Authors demonstrated that the binding of two inhibitors, rasagiline and isatin, to human MAO B I199F mutant enzyme is identical to that of WT enzyme. In both cases, the side chain of Phe199 extends into the entrance cavity with essentially identical conformations rather than the 'open/closed' conformations seen with Ile199. In the same paper, the authors pointed out that the presence of this bulky residue in the entrance cavity does not appear to alter the kinetic properties of the enzyme or the binding affinity of a small competitive inhibitor.
48. Jorgensen, W. L.; Chandrasekhar, J.; Madurs, J.; Impey, R. W.; Klein, M. L. *J. Chem. Phys.* **1983**, *79*, 926–935.
49. Ryckaert, J. P.; Ciccotti, G.; Berendsen, H. J. C. *J. Comput. Phys.* **1977**, *23*, 327–333.